



HAL
open science

**High nonlinear urban ground motion in
Manila(Philippines) from 1993 to 2010 observed by
DInSAR: implications for sea-level measurement**

Daniel Raucoules, Gonéri Le Cozannet, Guy Wöppelmann, Marcello de
Michele, Médéric Gravelle, Arturo Daag, Marta Marcos

► **To cite this version:**

Daniel Raucoules, Gonéri Le Cozannet, Guy Wöppelmann, Marcello de Michele, Médéric Gravelle, et al.. High nonlinear urban ground motion in Manila(Philippines) from 1993 to 2010 observed by DInSAR: implications for sea-level measurement. *Remote Sensing of Environment*, 2013, 139, pp.386-397. 10.1016/j.rse.2013.08.021 . hal-00863850

HAL Id: hal-00863850

<https://hal.science/hal-00863850>

Submitted on 20 Sep 2013

HAL is a multi-disciplinary open access archive for the deposit and dissemination of scientific research documents, whether they are published or not. The documents may come from teaching and research institutions in France or abroad, or from public or private research centers.

L'archive ouverte pluridisciplinaire **HAL**, est destinée au dépôt et à la diffusion de documents scientifiques de niveau recherche, publiés ou non, émanant des établissements d'enseignement et de recherche français ou étrangers, des laboratoires publics ou privés.

1 **High nonlinear urban ground motion in Manila (Philippines) from 1993 to 2010**
2 **observed by DInSAR: implications for sea-level measurement**

3
4
5 Raucoules, Daniel^{a*}; Le Cozannet, Gonéri^a; Wöppelmann, Guy^b; de Michele, Marcello^a; Gravelle,
6 Médéric^b; Daag, Arturo^c; Marcos, Marta^b

7
8 ^a*BRGM, 3 av. Claude Guillemin, 45060 Orléans, France*

9 ^b*LIENSs, Université de La Rochelle - CNRS, 2 rue Olympe de Gouges, 17000 La Rochelle, France*

10 ^c*Philippine Institute of Volcanology (Phivolcs), PHIVOLCS Building, CP Garcia Avenue, U.P. Campus Diliman,*
11 *Quezon City 1101, Philippines*

12 **corresponding author: d.raucoules@brgm.fr; phone: 33-2 38 64 30 86*

13
14
15 **Keywords:** DInSAR; subsidence; sea level rise estimation; Manila

16
17 **Highlights:**

- 18
19 - Differential SAR interferometry has been applied in Manila (Philippines)
20 - High nonlinear ground motion was observed during 1993–1998 and 2003–2010.
21 - A comparison with independent ground-level measurements (GPS, DORIS, and Tide Gauge) was
22 carried out.
23 - The consequences for sea-level estimation were analyzed using a local tide gauge and GPS
24 station.
25

26
27 **ABSTRACT:**

28 In coastal low-lying urban areas, vertical ground motions can significantly exacerbate the hazards related to
29 sea-level rise. However, their spatial extent, their temporal evolution, and even sometimes their existence
30 are often poorly known. This study aims to monitor variable urban ground motion (uplift and subsidence)
31 from 1993 to 2010 in the metropolitan area of Manila, Philippines. Because high subsidence rates have
32 been reported in this city in previous studies, conventional differential SAR interferometry (DInSAR) was
33 applied with an adapted stacking procedure to the archive of ERS and Envisat satellite images to produce
34 surface deformation-velocity maps for different periods. The results showed that the city is locally affected

35 by vertical ground motions on the order of 15 cm/yr. Moreover, the spatio-temporal evolution of the ground-
36 motion phenomena is highly nonlinear. These results are in good agreement with previous studies focused
37 on groundwater use in Manila and in the Marikina Fault Valley, suggesting a plausible interpretation of the
38 processes causing surface motion. Incidentally, the ground motions are affecting the locations of several
39 geodetic instruments, including a tide gauge with sea-level records starting in 1902, two permanent GPS
40 (Global Positioning System) stations, and a DORIS (Doppler Orbitography and Radiopositioning Integrated
41 by Satellite) station. A major implication of those large and locally variable ground motions is that they
42 impede the use of the nearby GPS and DORIS data to correct the tide-gauge records and to derive robust
43 sea-level trends associated with climate change.

44

45 1. Introduction

46 As sea level rises, there is increased concern about the growing urbanization of the world's coastal zones
47 and the related coastal hazards, particularly in Southeast Asia (McGranahan *et al.*, 2007; Nicholls &
48 Cazenave, 2010). However, climate-induced sea-level rise is not the only process leading to changes in
49 mean relative sea levels in coastal cities: the local relative sea-level rise (i.e., as experienced on the coast)
50 can be significantly affected by vertical ground motions, subsidence or uplift, either due to natural
51 processes (e.g., global isostatic adjustment, tectonics, sediment compaction) or to human activities (e.g.,
52 groundwater pumping, hydrocarbon extraction).

53

54 In a recent assessment of the exposure of the world's coastal cities to coastal submersion hazard, Hanson
55 *et al.* (2011) have highlighted that subsidence or uplift (1) affects many important coastal cities worldwide
56 and (2) can be in the same order of magnitude or greater than climate-induced sea-level rise. It is therefore
57 important to take into account these processes for evaluating how changes in sea level may affect coastal
58 cities in the future. However, while coastal ground motions are recognized important, they are in practice
59 often poorly known. In many cases, little information is available about the processes that generate ground
60 motion (e.g., location and rates of groundwater pumping) and on ground-motion patterns. In addition,
61 vertical ground motions often reveal strong spatial and temporal variability, so that their mapping is a
62 complex task.

63

64 As a complement to *in-situ* monitoring (e.g., using GPS or leveling), space-borne Differential Synthetic
65 Aperture Radar Interferometry (DInSAR) provides a means to deliver a comprehensive mapping of surface
66 deformation (e.g., Brooks *et al.*, 2007; Lagios *et al.*, 2006; Raucoules *et al.*, 2008; Bock *et al.*, 2012;
67 Chaussard *et al.*, 2013). The principle of DInSAR is to infer ground-motion displacements from the
68 evolution of the phase of space-borne Synthetic Aperture Radar between two or more satellite passes.
69 Although the technique encounters limitations in vegetated areas, it can be applied efficiently in urban
70 environments. In addition, provided that the displacements are not too rapid given the geometric and
71 temporal characteristics of the available SAR scenes time series, the method has been shown to be
72 efficient for monitoring slightly nonlinear ground motions (e.g., Kim *et al.*, 2010).

73
74 Using SAR data acquired by the ERS and Envisat satellites from 1993 to 2010, this study uses DInSAR to
75 monitor ground motions affecting Manila, on Luzon Island in the Philippines. Located on a coastal
76 floodplain between the eastern part of Manila Bay and Laguna de Bay, the Manila metropolitan area is
77 considered to be highly vulnerable to the adverse effects of flooding and of sea-level rise (World Bank,
78 2010). The 2010 population census reported that Manila has a population of 11.8 million inhabitants
79 (National Statistics Office, Republic of the Philippines, 2010). In addition, previous studies have reported
80 that the city is subject to ground motions: as the population has grown, water demand and groundwater
81 extraction have drastically increased (Clemente *et al.*, 2001), causing ground surface motions in the city of
82 Manila, as well as in other locations around Manila Bay (Siringan & Ringor, 1998; Rodolfo & Siringan,
83 2006; Daag *et al.*, 2011, Clemente *et al.*, 2001). Finally, the eastern part of the city is crossed by a seismic
84 fault, the Marikina Fault Valley (Rimando & Knuepfer, 2001).

85
86 Interestingly, the city hosts several important geodetic instruments which are potentially useful for
87 estimating contemporary sea-level rise. Tide-gauge measurements have been recorded in Manila since
88 1902, which makes this the longest time series in Southeast Asia. Therefore, this gauge belongs to the
89 “Global Core Network” of the Global Sea Level Observing System (GLOSS). However, the tide gauge is
90 suspected of being affected by ground motions, presumably due to groundwater withdrawal, at least since
91 the 1950s (Santamaría Gómez *et al.*, 2012). To correct sea-level time series from these ground motions
92 (as proposed by Wöppelmann *et al.*, 2007), several geodetic instruments located in metropolitan Manila
93 might be used: two GPS stations and a DORIS (Doppler Orbitography and Radiopositioning Integrated by

94 Satellite) station (Willis *et al.*, 2010). However, these instruments are located several kilometers away from
95 the tide gauge (Fig. 1). Because no repeated leveling surveys are presently available in the GLOSS data
96 repositories (www.sonel.org; www.psmsl.org), it is unknown whether the location of these instruments has
97 been affected by the ground-motion processes.

98
99 In this study, DInSAR is applied to the Manila urban area with the objective of providing preliminary
100 answers to the following questions:

- 101 (1) What was the spatial and temporal variability of ground-surface deformations in Manila from 1993
102 to 2010?
- 103 (2) To which extent do these deformations affect the locations of the tide gauge and of the GPS and
104 DORIS stations?
- 105 (3) What are the possibilities for using sea-level time series before 1993 in Manila?

106
107 The paper proceeds as follows: Part 2 describes the data and the DInSAR processing. Part 3 reports on
108 the observations of surface deformations and provides preliminary interpretations in relation to previous
109 studies focused on groundwater extraction and on the Marikina Valley Fault. Finally, in Part 4, the paper
110 discusses to which extent the combination of permanent GPS measurements and DInSAR is able to
111 provide correction for long-term tide-gauge time series for this particular site, considering the high observed
112 deformation rates and their irregular temporal evolution.

113
114
115

116 2. Processing procedures and data

117 2.1 Choice of an adapted DInSAR processing procedure

118
119 Several DInSAR algorithms can be used for processing SAR data, from conventional DInSAR (e.g.,
120 Massonnet and Feigl, 1998), possibly with an adapted stacking procedure (e.g., Usai *et al.*, 2003) to
121 advanced techniques such as Persistent Scatterers Interferometry (PSI, e.g., Ferretti *et al.*, 2000;
122 Wegmuller *et al.*, 2004) or Small Baseline Subsets (SBAS, e.g., Pepe *et al.*, 2005). The quality of the

123 results obtained by each method can vary widely depending on the area of interest and on the available
124 SAR images. In places such as the densely urbanized Manila metropolitan area, conventional DInSAR
125 often provides interferograms with good coherence even over large time spans (a few years), provided that
126 the perpendicular baselines are not too high. However, these interferograms are affected by atmospheric
127 effects, typically leading at the spatial wavelength of this study (~20 km) to errors of the order of one
128 centimeter, but in certain cases to errors larger than a fringe (e.g., Hanssen, 2001). When a sufficient
129 number of SAR scenes have been acquired, stacking procedures can average and reduce atmospheric
130 effects, which are supposed to be spatially correlated and temporally uncorrelated. With this assumption,
131 uncertainty due to atmosphere is reduced as the inverse of \sqrt{N} , where N is the number of independent
132 interferograms (Zebker *et al.*, 1997; Peltzer *et al.*, 2001). For the presented results, that corresponds to
133 approximately 4 mm/yr for the ERS data set (with only thirteen images) and better than 1 mm/yr for the
134 EnviSat/ASAR data set.

135 Stacking procedures are relatively easy to use and can often provide information about potentially
136 nonlinear ground motions in the order of a few centimeters per year (e.g., Le Mouelic *et al.*, 2005). Finally,
137 advanced techniques such as PSI can be efficient if PS density is sufficient and can reach high precision.
138 However, in the case of spatially and temporally variable rapid ground deformations, PSI techniques (in the
139 standard procedure based on the use of linear or slightly nonlinear displacement evolution models) can be
140 affected by spatial and temporal unwrapping errors that result in underestimation of the velocity and
141 incorrect atmospheric phase screen estimation (Raucoules *et al.*, 2009). When no prior information on
142 patterns of urban ground deformations is available, stacking procedures are easily applicable and can
143 provide maps of vertical ground motions. This approach was selected for the case study in Manila.
144 Combinations of ascending and descending modes can in certain cases (e.g., Wright *et al.*, 2004) be used
145 for separating vertical motions other than horizontal (in fact, mostly East-West because of the orbital
146 orientation). However, in the study area, the data archive in ascending mode is insufficient (in fact only one
147 ASAR pair is archived) to derive deformation maps for the period of interest. Assumptions on the direction
148 of motion are therefore needed for interpretation.

149

150 2.2 Description of data and processing

151

152 Using a series of ERS 1-2 images between 1993 and 2000 (Table 1) and ASAR/EnviSAT data between
 153 2003 and 2010 (Table 2), differential interferograms having perpendicular baselines shorter than 300 m
 154 were processed. Then, as suggested, e.g., by Le Mouelic *et al.*, (2005), a subset of trustworthy
 155 interferograms was selected visually by rejecting noisy phases and data obviously affected by atmospheric
 156 effects. In addition to rejecting low-coherence interferograms, the interferograms were compared by pairs
 157 to identify obvious atmospheric effects. Figures 2a and 2b show the selected interferograms and related
 158 acquisition times and perpendicular baselines. Deformation is assumed (even for nonlinear deformation) to
 159 have a certain temporal correlation, whereas atmosphere turbulence is assumed uncorrelated. By
 160 identifying similarities and dissimilarities on the interferograms, it was possible to detect acquisitions
 161 affected by strong atmospheric effects that could severely impair a stacking result. Finally, interferograms
 162 were stacked for the entire observation periods [1993–1998 (ERS) and 2003–2010 (Envisat)] and for sub-
 163 periods of three years. We focused on time spans shorter than 400 days to avoid unwrapping errors in
 164 interferograms with more than five or six fringes and to limit temporal decorrelation. Note that the ERS
 165 acquisition for 2000 does not allow production of interferograms meeting the requirements in terms of time
 166 span.

167 This processing was carried out using the GAMMA interferometric software (Wegmuller *at al.*, 1998).

168
 169 2.3 Specific procedures for analyzing temporally variable ground motions and fault-related
 170 deformations

171
 172 In addition, a principal components analysis (PCA) was performed on the deformation maps to discriminate
 173 the areas affected by constant deformation (first component) from those affected by time-varying
 174 deformation. Finally, a directional filter was computed for the 2003–2010 deformation maps of the Marikina
 175 Valley Fault area (east of Manila) to locate sections of the fault affected by surface motion.

176
 177 Table 1: ERS 1–2 acquisitions (track 418)

Year	Acquisition dates
1993	25 July, 29 Aug, 3 Oct
1995	4 April, 13 June, 31 Oct, 5 Dec
1996	9 Jan, 19 March, 11 Sept

1997	1 Oct, 5 Nov
1998	14 Jan
2000	23 Feb

178 Mean incidence angle: approximately 23°

179

180

181

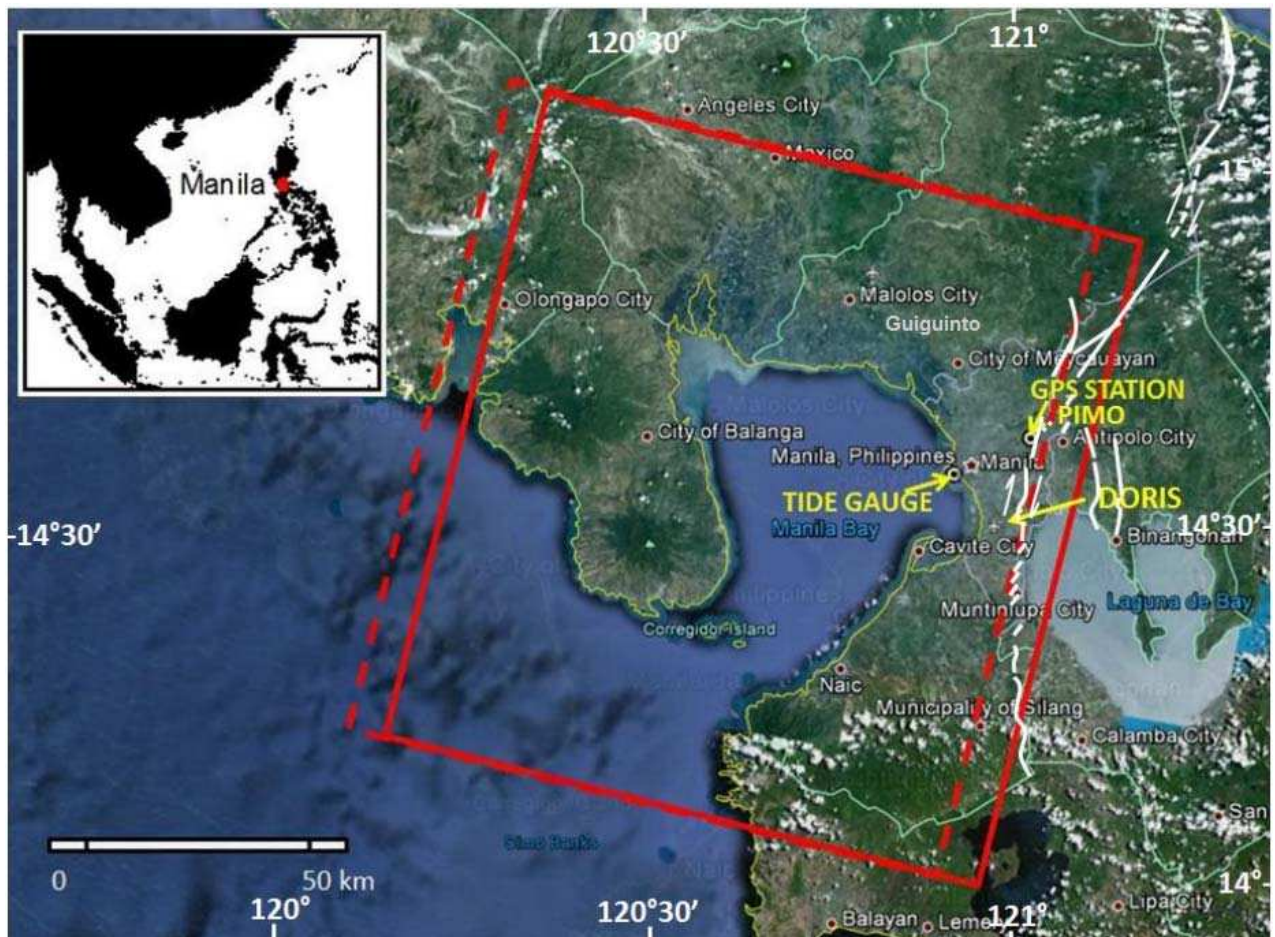
182 Table 2: EnviSat/ASAR acquisitions (track 418)

Year	Acquisition dates
2003	8 Jan, 12 Feb, 19 March, 2 July, 10 Sept, 24 Dec
2004	28 Jan, 3 March, 12 May, 21 July, 25 Aug, 29 Sept, 3 Nov, 8 Dec
2005	12 Jan, 16 Feb, 23 March, 27 April, 1 June, 6 July, 10 Aug, 14 Sept, 28 Dec
2006	1 Feb, 8 March, 12 April, 17 May, 26 July, 17 Jan, 26 July
2007	17 Jan, 24 Oct, 28 Nov
2008	12 March, 25 June, 3 Sept, 12 Nov
2009	21 Jan, 2 Dec
2010	4 Aug

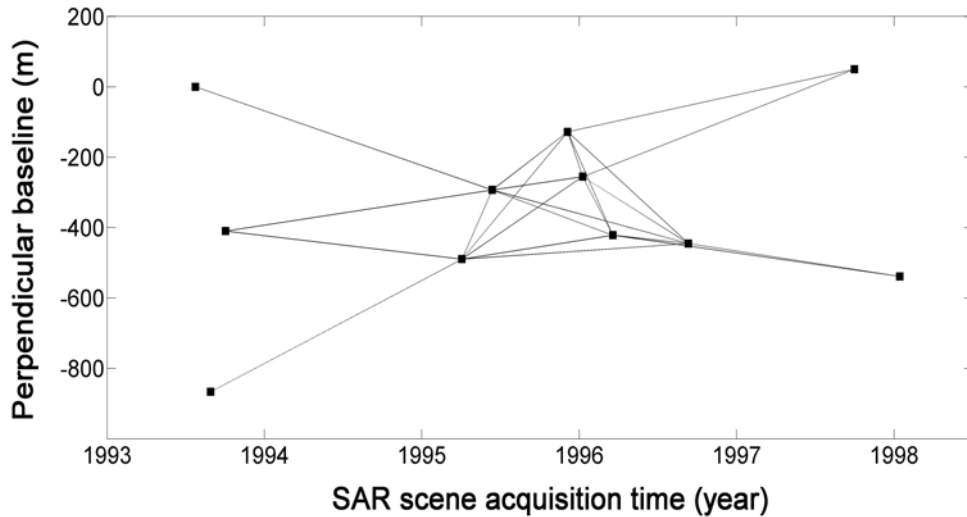
183 Mean incidence angle: approximately 23°

184

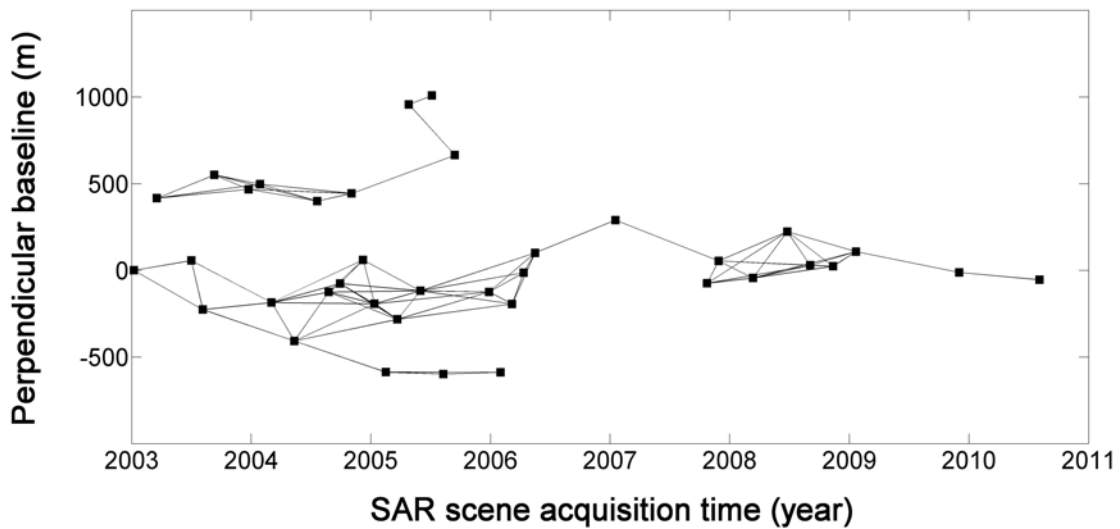
185



186 *Figure 1: Location of the Manila metropolitan area. This map shows (1) the area covered by the SAR data*
 187 *acquisition frames on Manila Bay, with solid lines corresponding to the ASAR/ENVISAT acquisitions and*
 188 *dashed lines to ERS 1 and 2 data; (2) the position of the Marikina Valley Fault System (MVFS), based on*
 189 *Rimando & Knuepfer, (2006); the ASAR data cover part the Marikina Valley Fault, whereas the ERS data*
 190 *do not due to a slight westward shift of ERS; (3) the location of the tide gauge, GPS (PIMO), and DORIS*
 191 *stations; the MANL GPS station is located close to the tide gauge (see Fig. 3a), but no reliable vertical*
 192 *velocity could be computed for the study period using the SONEL data repository (www.sonel.org).*
 193



194
 195 *Figure 2a: Baseline/time diagram for the ERS 1/2 data. The interferograms used for the study (those that*
 196 *met the requirements in terms of baseline and time span) are represented by vectors with coordinates*
 197 *corresponding to their baselines and time spans. The zero perpendicular baseline refers to the scene*
 198 *acquired on July 25, 1993.*
 199



200
 201 *Figure 2b: Same as Figure 2a for the EnviSAT/ASAR data. The zero perpendicular baseline refers to the*
 202 *scene acquired on January 8, 2003.*

203
 204
 205 **3. Results: observations and preliminary interpretations**

206

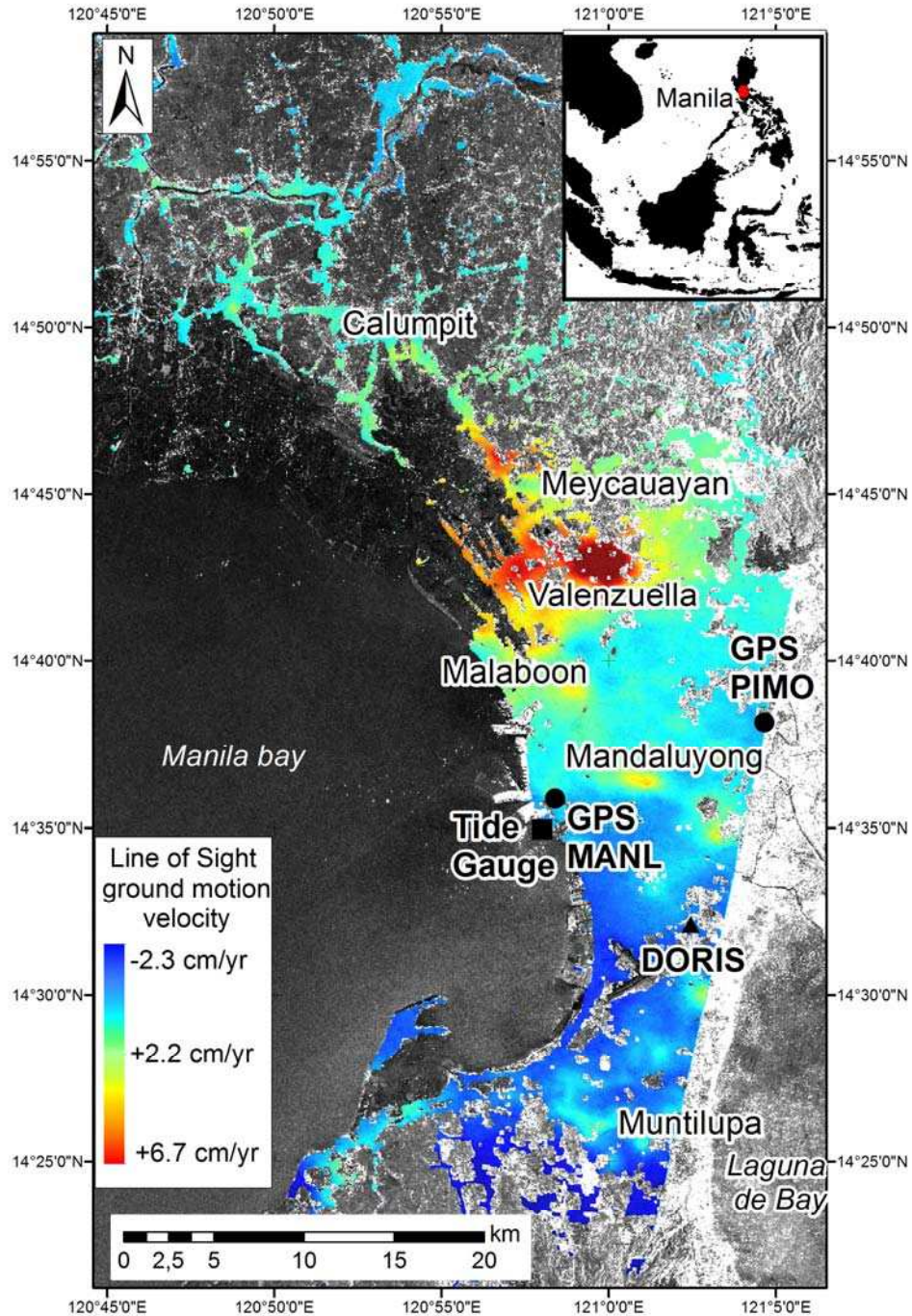
207 3.1 Velocity maps

208 Deformation maps were produced as shown in Figs. 3 and 4. The scale corresponds to Line of Sight (LOS)
209 in cm/yr. Because of the 23° view angle of the acquisition geometry, the LOS measurement is 2.3 more
210 sensitive to the vertical component of the displacement than to the horizontal. The horizontal component of
211 the subsidence displacement is generally much smaller than the vertical, but in certain cases could be non-
212 negligible with respect to the vertical, although smaller (e.g., for coal-mining subsidence, the ratio between
213 the maximum horizontal and the maximum vertical components is approximately 0.4; Tandanand & Powell,
214 1991). On the basis of these two observations, it can be assumed that for subsidence, the measured LOS
215 component is related mostly to the vertical component of the displacement. Under this assumption, 10
216 rad/yr would correspond to approximately 4.9 cm/yr of vertical motion. However, horizontal displacements
217 probably occur in the Marikina Valley Fault because it is mainly a strike-slip fault. In fact, if the observed
218 motion were mainly due to fault activity and not related to pumping-induced subsidence, the measured LOS
219 displacement would be the projection of an along-fault motion (except on sections of the fault having a
220 more complex motion).

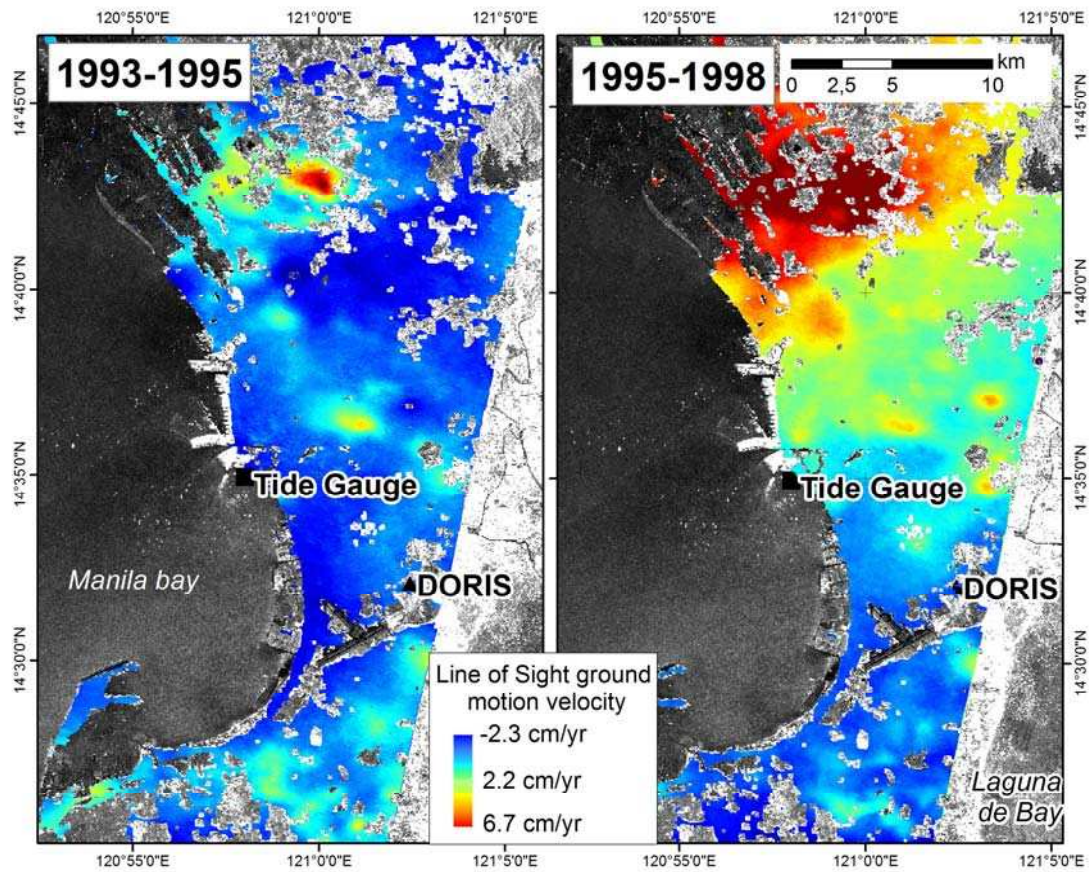
221 Pixels with an interferometric coherence less than 0.3 were considered unreliable and were used to define
222 a mask. Morphological operations (opening and closing) were applied to the mask to remove irregularities
223 before the mask was applied to the interferograms.

224 Because of the generalized surface motion in the area, it is difficult to find a reliable and stable reference
225 point. However, the DORIS instrument provides a local estimate of vertical velocity. The deformation maps
226 were corrected by a value (constant for a given map) to be compatible with the displacement observed by
227 DORIS for the corresponding period (and therefore to convert relative measurements from DInSAR in
228 absolute motion estimates). Values of the DORIS motion rates and a description of the data are given in
229 Section 4.1.

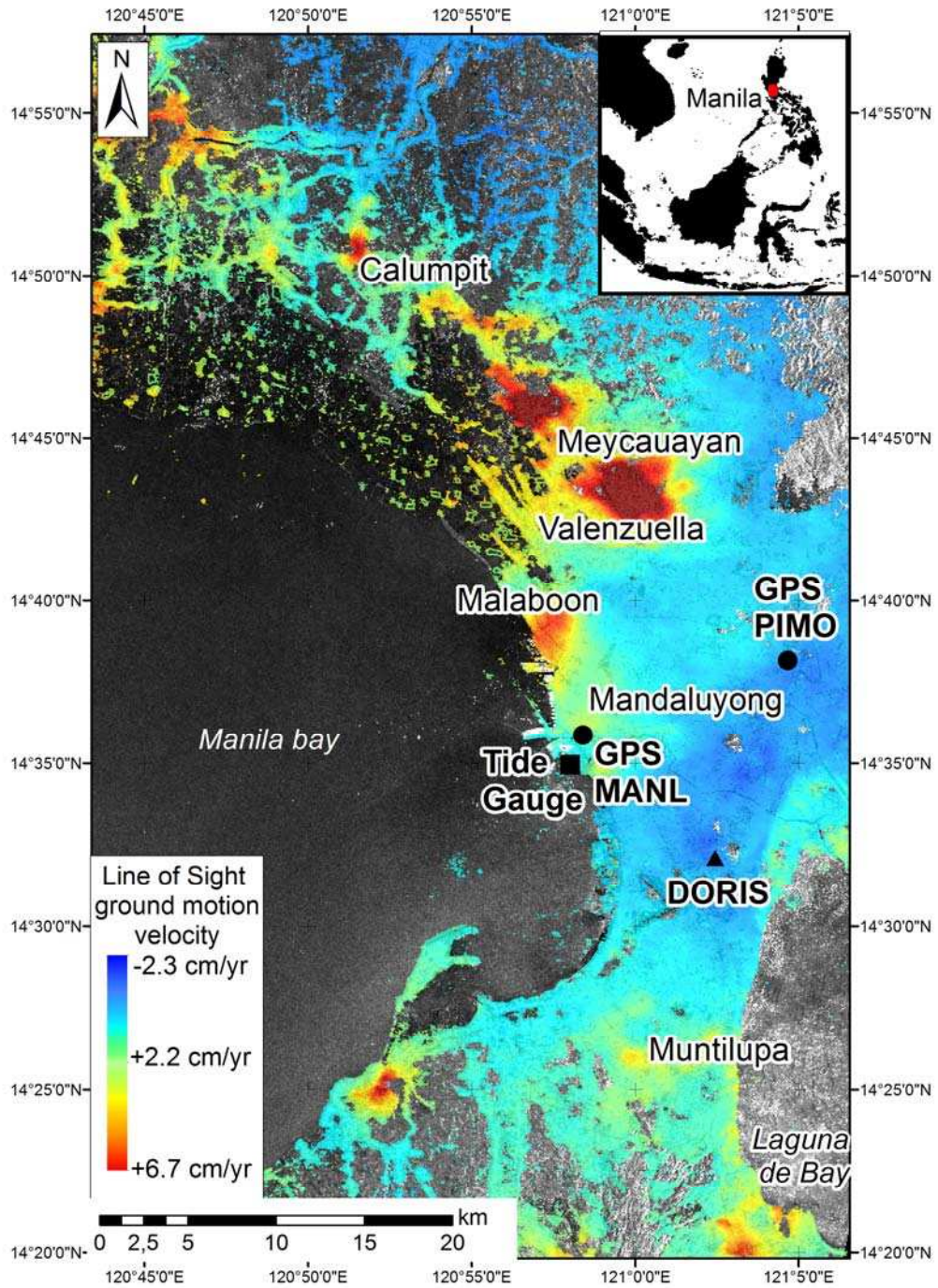
230



231
 232 *Figure 3a: Line of Sight ground motion velocity in cm/yr for the whole 1993–1998 period (ERS 1-2 data).*
 233 *Negative values correspond to displacements towards the sensor (i.e., uplift). For figure readability, the*
 234 *color palette in this figure and in the following velocity maps is saturated at its extreme values.*
 235



236
 237 *Figure 3b: Line of Sight ground motion velocity maps for 1993–1995 and 1995–1998. An increase in*
 238 *subsidence rate in the northern part of the city appears between 1995 and 1998.*



239

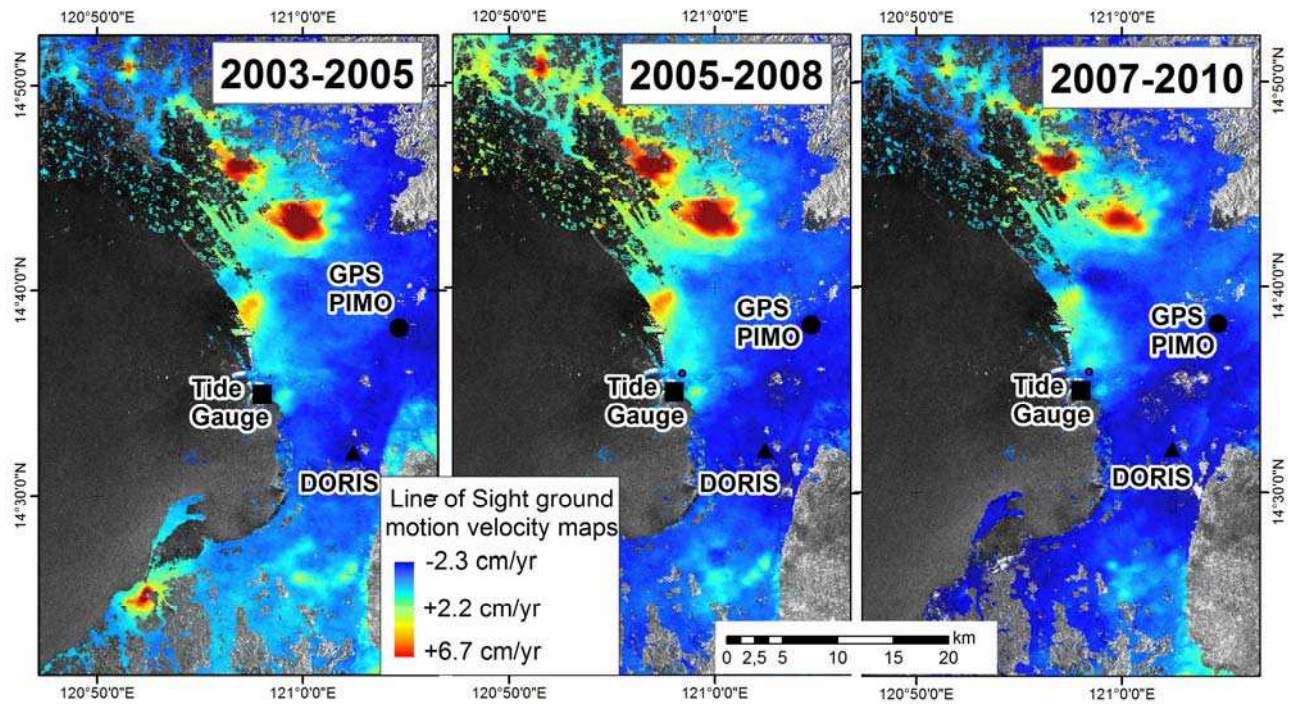
240

241

Figure 4a: Line of Sight ground motion velocity in cm/yr for the whole 2003–2010 period (EnviSat/ASAR

data).

243



244
 245 *Figure 4b: Line of Sight ground motion velocity maps in cm/yr for 2003–2005, 2005–2008, and 2007–2010*
 246 *(EnviSat/ASAR data).*

247
 248 The velocity maps reveal non-linear deformation rates. For example, Fig 3b indicates that the subsidence
 249 from 1995 to 1998 was quicker in the north-western part of Metro-Manila than from 1993 to 1995. How
 250 reliable is this result ? Due to the limited number of SAR images available from the ERS satellite, these
 251 velocities maps might be partly affected by atmospheric noise or by slight errors in orbit calculation and
 252 very large atmospheric effects at the scale of the imaged area might have resulted in tilts. In our approach,
 253 these tilts are corrected by removing tilts on each single interferogram (estimated using Fast Fourier
 254 Transforms) and then the possible residual tilts are minimized over the whole data set during the stacking
 255 procedure. While such errors are more difficult to correct when fewer SAR images are available, an
 256 analysis of individual interferograms confirms that the acceleration of subsidence is affecting the same area
 257 for several individual interferograms. This temporal correlation of interferograms as well as their velocity
 258 indicates that these non-linear velocities cannot only result from atmospheric noise, and confirm the
 259 acceleration of subsidence from 1995 to 1998 compared to 1993 to 1995. Nevertheless, for the ERS data
 260 set, we can consider the 1993-1998 map as more reliable than the two sub-sets (1993-1995 and 1995-
 261 1998), because more interferograms were stacked and because the DORIS velocity estimation better
 262 represents the average motion over the whole period. More SAR images are available from EnviSAT, thus

263 making the results in figure 4a and 4b more reliable. Several non-linear patterns can be observed in these
264 maps, such as the extension of a coastal subsidence southward in the direction of the tide gauge, or the
265 disappearance of a subsidence pattern on the southern shore of Manila Bay. These results therefore also
266 highlight the non-linearity of the urban subsidence process in Manila.

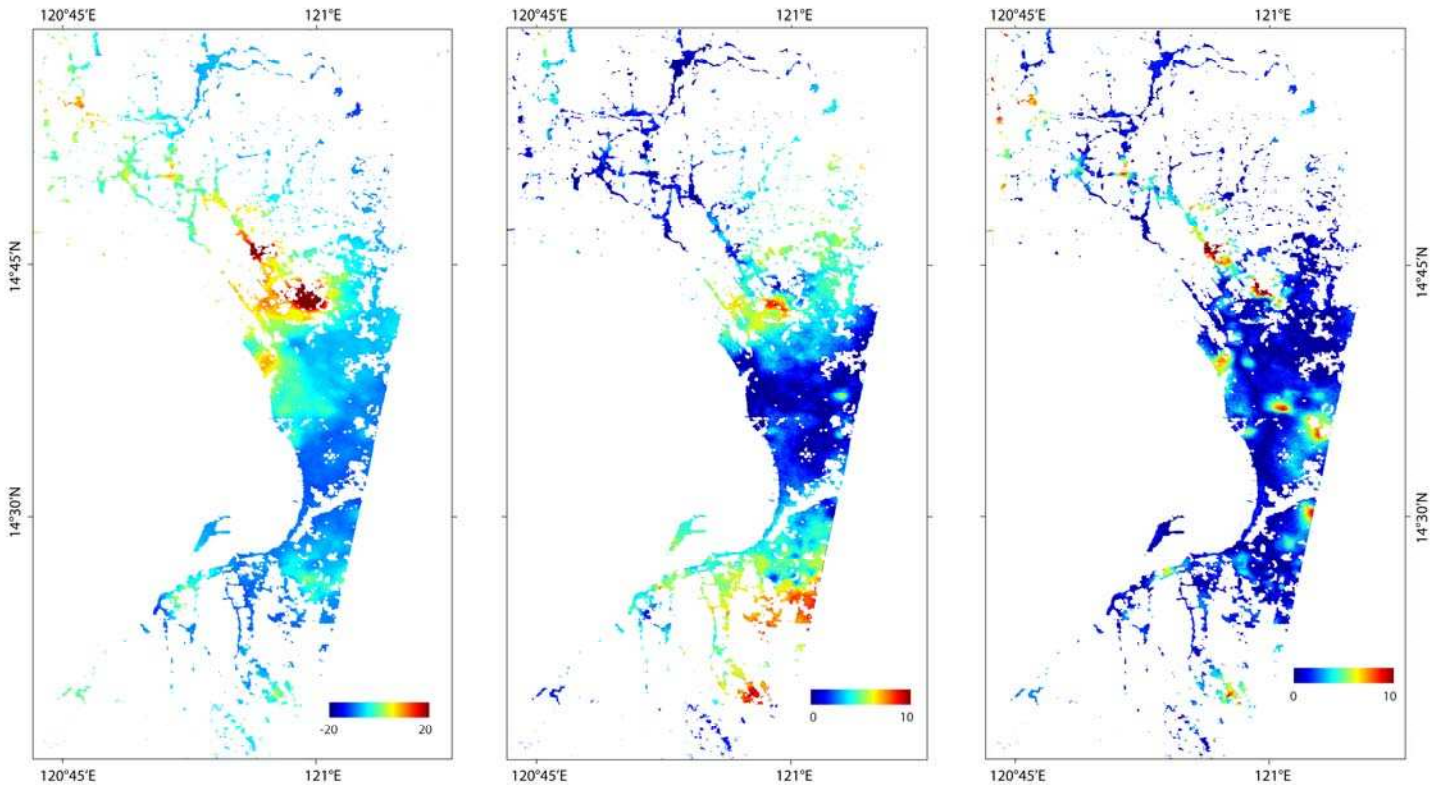
267 Velocity maps not only display non-linear patterns, but also high rates of deformations. For example,
268 deformation rates up to 13 cm/yr were observed in Valenzuela and Meycauayan and rates of approximately
269 9 cm/yr northwest of Guiguinto (note that for visual reason, we saturated the color palette to 6.7cm/yr). In
270 these sectors, deformation was much slower and spatially reduced between 1993 and 1995. The highest
271 deformation rates observed in Valenzuela and Meycauayan are visible on the 1995–1998 and 2003–2005
272 maps (a decrease of the phenomenon in this sector is visible on this last map with respect to the first one),
273 whereas a maximum was obtained after 2005 near Guiguinto.

274
275 Changes in the location and rates of groundwater extraction are a plausible explanation for this migration of
276 the deformation maxima. As reported by Clemente *et al.* (2001), groundwater pumping in Manila has been
277 multiplied by a factor of five since the 1970s because of population growth. This has resulted in a lowering
278 of the groundwater table by several tens of meters. The authors also suggest land subsidence as a
279 possible consequence of pumping. Clemente *et al.* (2001) provide piezometric maps which show that the
280 deformation maps generated in this study are consistent with the locations of very low water table levels in
281 the 1990s. For instance, they reported that groundwater was intensively extracted in Muntlupa and
282 Valenzuela, where high ground-motion velocities in the 90's were observed in this research. This suggests
283 that many ground deformations observed using DInSAR in this research are direct consequences of
284 groundwater pumping in the Manila metropolitan area.

285 286 3.2 Monitoring of Temporal Evolution of Ground Deformations through Principal 287 Components Analysis

288
289 Because the results showed strong temporal variability, a principal components analysis was carried out to
290 highlight areas subject to deformation-rate changes. The idea was to separate areas with constant
291 deformation rates from areas affected by nonlinear deformation components. Principal components
292 analysis (PCA) was therefore applied to the five deformation-rate maps corresponding to the different

293 periods studied. It was assumed that the first principal component (PC) was related to the common linear
294 deformation (the first component being highly correlated with all the initial deformation maps) and the
295 second and third components to nonlinear deformations which differ among the five maps (upper-order
296 components were neglected because the fourth eigenvalue was approximately one-twentieth of the first
297 one). The three first eigenvalues were $\lambda_1=43$, $\lambda_2=11$ and $\lambda_3=4.3$.
298



299
300
301 *Figure 5: Maps showing the three first principal components. For the second and third components, the*
302 *absolute values of the components are shown. Locations of the displacements are therefore identified by*
303 *this information rather than their evolution (acceleration, deceleration).*

304
305 Figure 5 highlights the observation that in addition to strong spatial variability, deformation patterns in
306 Manila show a complex temporal evolution. In particular, this figure indicates that in addition to the northern
307 part of the city (e.g., the area between Valenzuela and Meycauayan), the cities of Malaboon, Mandaluyong,
308 and Muntinlupa were affected by nonlinear deformations. Small areas spotted on the third component
309 deserve deeper investigation because temporal changes at short spatial wavelengths could have

310 implications such as damage to buildings. Actual links with pumping locations in these areas should be
311 investigated, for example by identifying whether localized velocity changes can be correlated with the
312 installation of new pumping facilities during the study period.

313

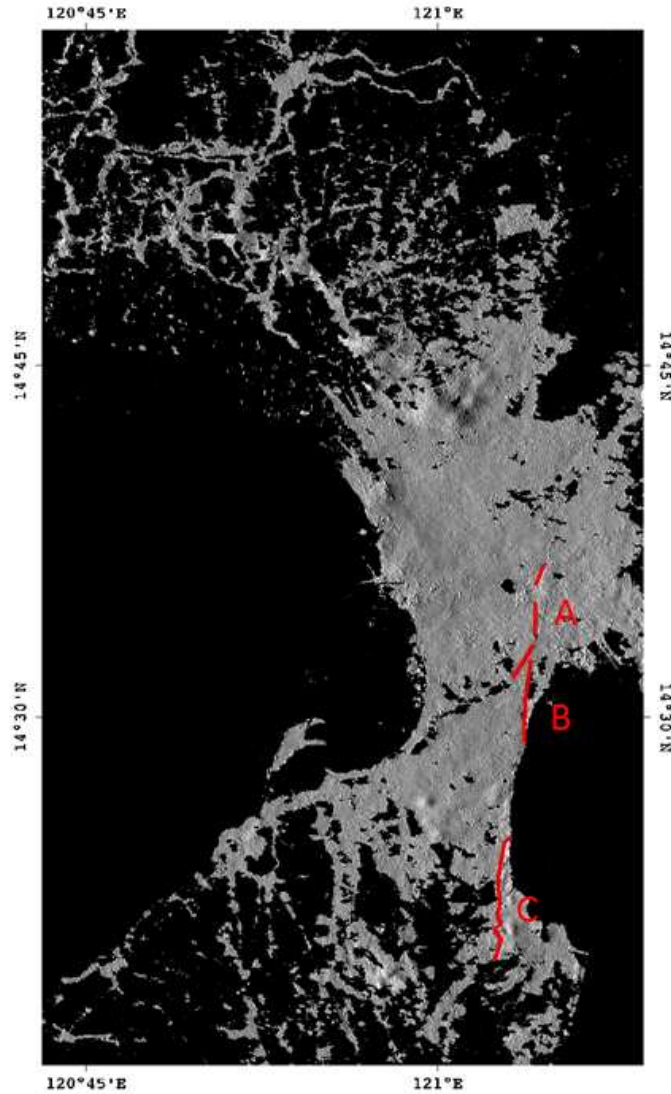
314 3.3 Deformation in the Marikina Valley Fault area

315

316 To investigate displacement along the Marikina Valley Fault, an east-west directional filter was used to
317 highlight differential motion between each side of the fault (Fig. 6). Basically, the filtered image consists of
318 an along-column (approximately across-fault) deformation first derivative for which the histogram has been
319 adjusted and the result rescaled to obtain arbitrary values distributed between zero and one. This
320 procedure aims to provide better identification of linear features (similarly to a shaded map) that could be
321 associated with fault motion. Sections of the fault that possibly moved between 2007 and 2010 were then
322 located. Note that the ERS frames did not cover the fault, and therefore this observation is based only on
323 the ASAR data. The 2007–2010 maps clearly show differential displacement along the fault (Fig. 4b).

324 The observed fault section was divided into three sections based on their motion characteristics: A and C:
325 west side moves towards the sensor faster than east side; B has the opposite behavior to A and C. On the
326 three sections, the differential LOS displacement (identified on the deformation map) corresponds to
327 approximately 5-15 mm/yr. Because the fault strike is oriented north-south, it can be assumed that pure
328 strike-slip motions have little influence on the deformation maps produced. Therefore, vertical motion must
329 dominate the signal. Based on this assumption, the observed motion corresponds to up to 8 mm/yr of
330 vertical displacement between the two sides of the fault. The source of this kind of motion is difficult to infer
331 based only on the DInSAR measures, which provide only one component of the deformation in three-
332 dimensional space. Deformation could be related either to tectonic strain (e.g., surface creep) or to
333 subsidence related to water extraction (as observed by Cigna *et al.*, 2011). In this case, the fault would act
334 as a natural barrier.

335



336
 337 *Figure 6: West-east directional filtering of the 2005–2010 deformation in arbitrary units. Bright areas*
 338 *correspond to the highest values of W-E derivatives. The red line corresponds to possible sections of the*
 339 *fault affected by differential displacement between the sides of the fault (located on linear features of the*
 340 *filtered map). The three sections are identified using their different displacement behaviors.*

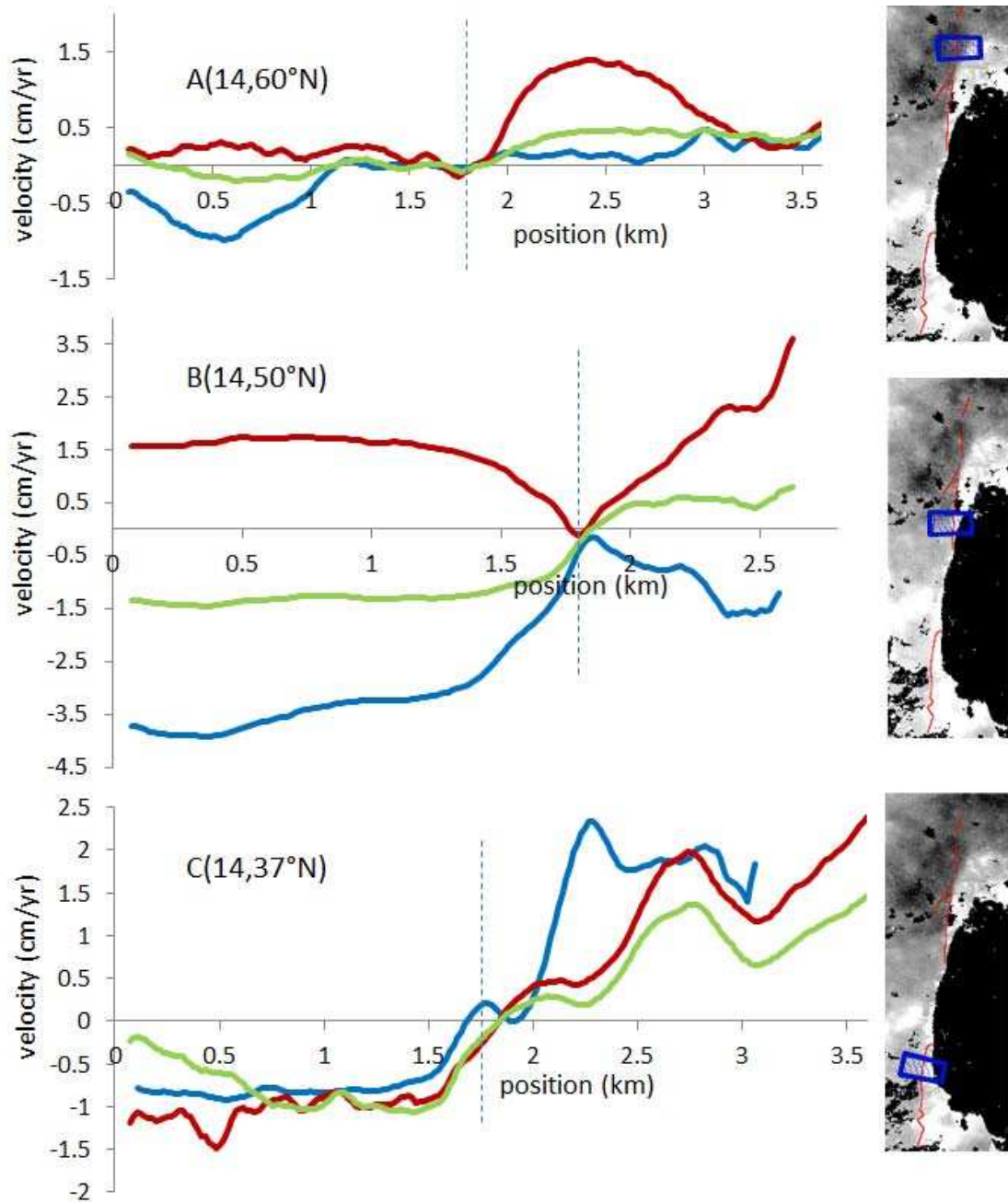
341
 342 A deeper analysis can be proposed. Based on both terrains offset measurements and magnitudes and
 343 recurrences of earthquakes, Rimando & Knuepfer (2006) have suggested that on the Rodriguez-Taguig
 344 segment (corresponding to sections A and B in this paper), the slip rate should be approximately 7–10
 345 mm/yr and should be mostly horizontal. They observed that the ratio between vertical and horizontal
 346 components of offsets is approximately 0.1. Considering the orientation of the fault with respect to the
 347 satellite-orbit path angle (between 0° and 12°) and the SAR incidence angle (approximately 23°), 10 mm/yr

348 of horizontal motion would result in approximately 0.8 mm/yr change in the LOS direction. This value is too
349 small to be measured by DInSAR. Therefore, non-tectonic subsidence seems more likely to be the cause
350 of the SAR signal for these sections. Section C of the fault (the Sucat-Binan segment) is characterized by
351 *en-echelon* elements. According to the authors, this segment is creeping, but they do not provide rate
352 estimations. This complicated behavior is not incompatible with vertical motion; the hypothesis that the
353 DInSAR observation shows creeping phenomena for this section cannot be rejected, but further dedicated
354 analysis would have to be performed to assess fault motion in this area.

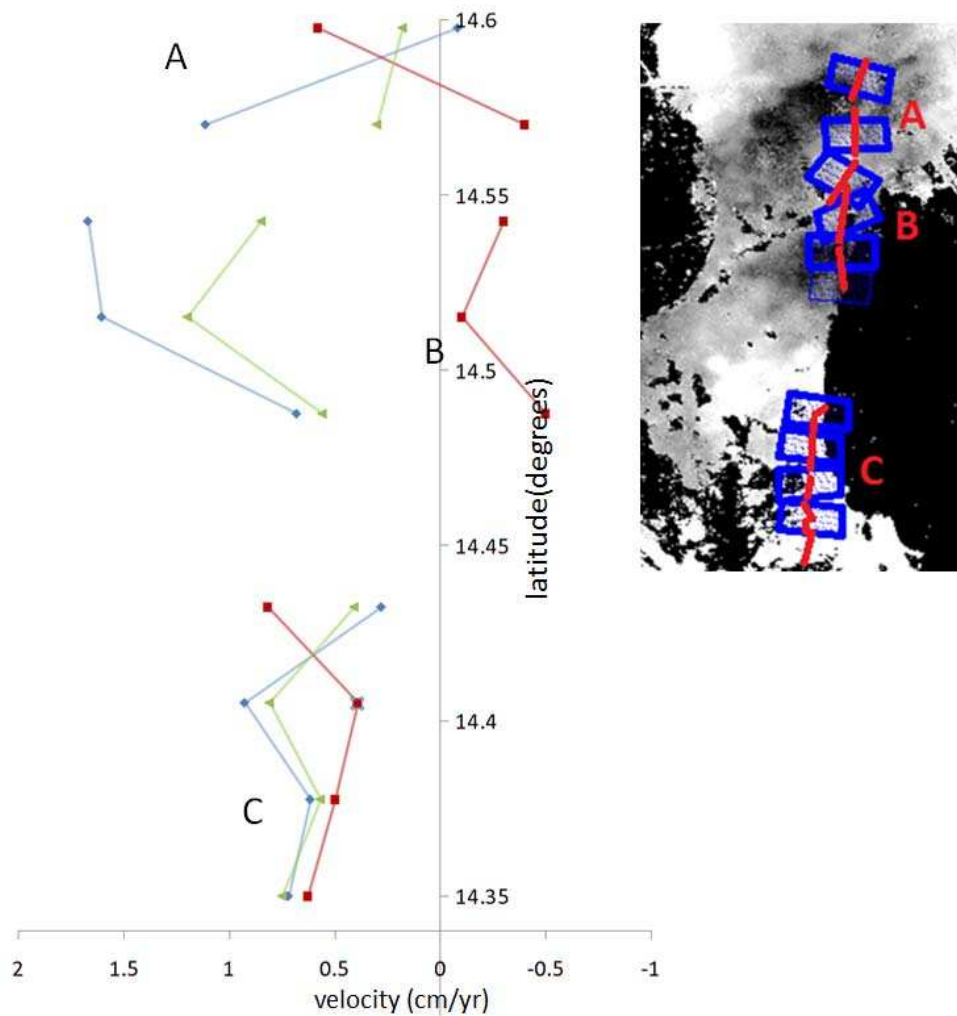
355
356
357 Figures 7 and 8 show profiles and estimations of the relative displacements between each side of the fault
358 using a 200-pixel length and stacked on 100 pixels width based on the COSI-Corr tools (for details on
359 these tools and a discussion of their reliability and precision, refer to Ayoub *et al.*, 2009). These figures
360 show that on sections A and B, the recorded LOS displacements are variable with time (including an
361 inversion of the motion for section B). On the other hand, on section C, the LOS motion is fairly stable at
362 approximately 6 mm/yr velocity (with a dispersion of approximately 2 mm/yr). These observations are
363 compatible with the fact that the fault mechanism is mainly N-S oriented strike-slip on A and B (blind to
364 DInSAR), and therefore the recorded vertical component of the motion must be due mainly to (variable)
365 non-tectonic causes. Section C, with its *en-echelon* structure, is known to creep (Rimando & Knuepfer,
366 2006). Therefore, this research might have measured the vertical component of fault creep in this area.

367

368



369
 370 *Figure 7: Relevant deformation across-fault profiles for each section: LOS velocities are given in cm/yr and*
 371 *the position in km (positive from west to east). These profiles are along fault stacks of 100 profiles 200*
 372 *pixels in length (profile length: approximately 3.6 km) according to the procedure implemented in the COSI-*
 373 *Corr tool (Leprince et al., 2007; Ayoub et al., 2009). The fault is approximately located, based on the*
 374 *directional filtering results, by the vertical dashed lines. In blue: profile derived from the 2003–2005 stack; in*
 375 *red, 2007–2010; in green, 2003–2010 The insets show the location of the profile stacks with respect to the*
 376 *fault.*
 377



378
 379 *Figure 8: Differential LOS velocity for the sides of the fault (west side with respect to east side) versus*
 380 *position on the fault (latitude). Velocities were obtained using the COSI-Corr tool. The 2003–2005 estimate*
 381 *(in blue) is compared to that for 2007–2010 (in red) and 2003–2010 (green). Section C shows a*
 382 *homogeneous behavior (vertical displacement of approximately 4–8 mm/yr), but the other sections show a*
 383 *more temporally variable evolution (sign change) not compatible with creeping phenomena. The inset*
 384 *shows the location of the profile stacks with respect to the fault.*

385

386

387 4. Discussion

388

389 4.1 Comparison with *in-situ* observations

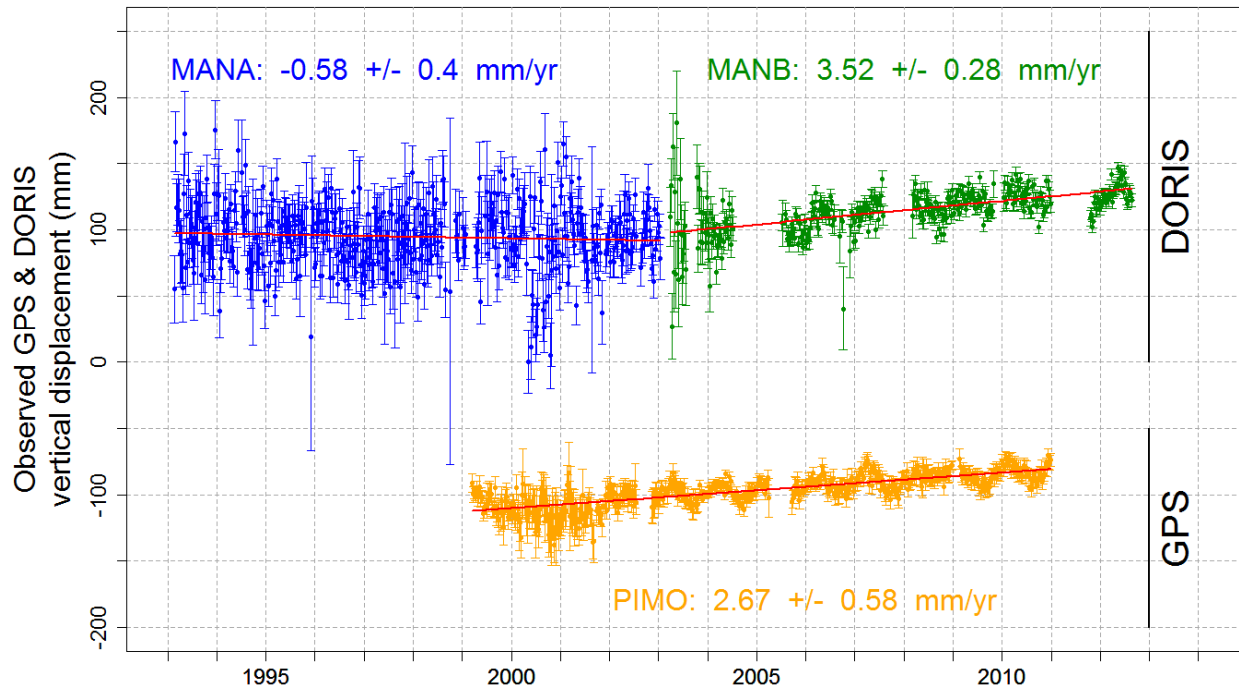
390

391 While no leveling surveys are presently available in global data repositories (Santamaría-Gómez et al.,
392 2012), a few geodetic instruments enable comparing our InSAR results with in-situ observations. These
393 geodetic instruments in Manila can be located on Fig. 2a. However, one permanent GPS station (GPS
394 MANL) provided a time series too short to be analyzed at the time of this study. As can be seen in Fig. 9
395 (blue), the DORIS instrument was nearly stable in average in the 1990s, but was affected by uplift in the
396 2000s (Fig. 9, green).

397 The GPS PIMO station was also subject to a slight uplift in the 2000s (Fig. 9, yellow). The differential
398 movement between PIMO and DORIS was consistently too small to be observed with DInSAR. During
399 2003–2010, the differential displacement between PIMO and the tide gauge (TG) as estimated from
400 DInSAR was approximately 10.7 mm/yr +/- 2.1 mm/yr, based on the sum of the variances of the DInSAR
401 deformation-rate measurements obtained on 200 m windows around the PIMO and TG locations. Once
402 corrected using the GPS absolute vertical motion, the resulting TG motion with respect to the reference
403 ellipsoid was approximately 8 mm/yr of subsidence (+/- 2.2mm/yr). To validate this result, the difference
404 between the sea-level variation recorded by AVISO data (Archiving, Validation and Interpretation of
405 Satellite Oceanographic data) and the TG data (Fig. 10) was calculated. The altimetric monthly sea-level
406 anomalies were obtained from the AVISO data server (<http://www.aviso.oceanobs.com/en/altimetry.html>).
407 These data are a multimission product (Jason 1-2, Envisat, Cryosat) with a spatial resolution of
408 0.25°x0.25°, starting in 1992. They include all geophysical corrections, in particular the dynamic
409 atmospheric correction that accounts for the effects of atmospheric pressure and wind (Volkov *et al.*, 2007).
410 To compare the tide-gauge data with the altimetry observations, this correction was added back in. The
411 most highly correlated grid point of the altimetry observations was chosen for comparison with *in-situ*
412 observations (the correlation was computed using de-seasoned and de-trended time series). Alternatives
413 such as the closest grid point or an average among nearby grid points around 1° did not change the
414 results. The combination of the altimetric observations with the tide-gauge data highlights subsidence of up
415 to 10.1 mm/yr +/- 0.6 mm/yr.

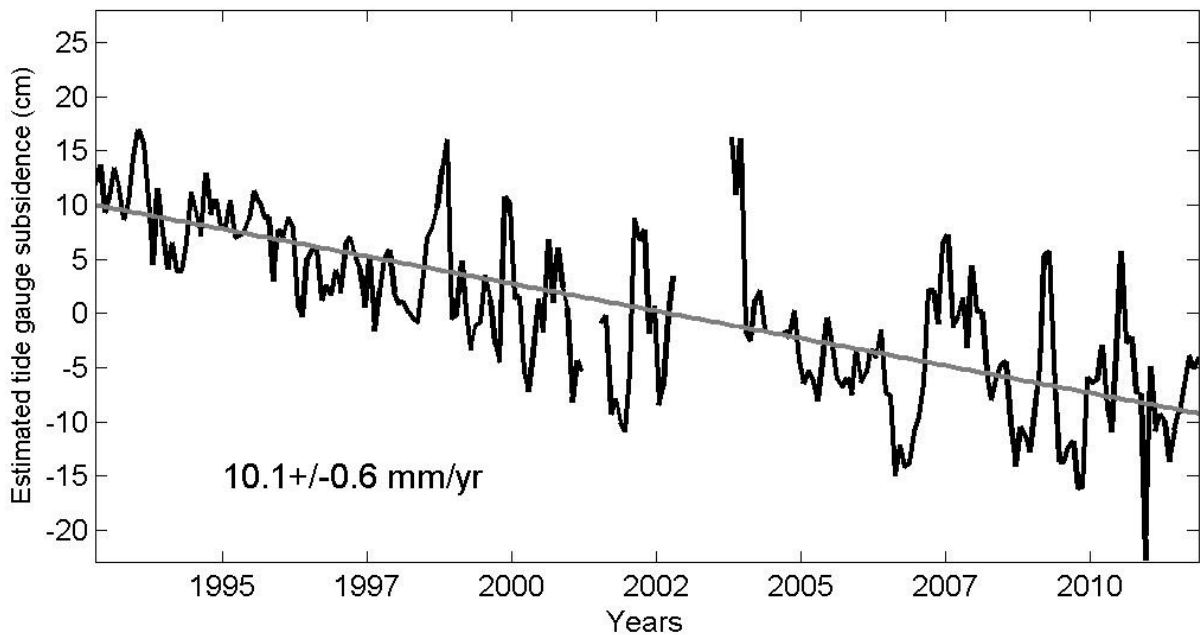
416
417 Finally, in addition to the multi-annual ground motion variability observed by DInSAR, the GPS time series
418 also revealed seasonal vertical deformations with an amplitude of approximately 5.5 mm.

419
420



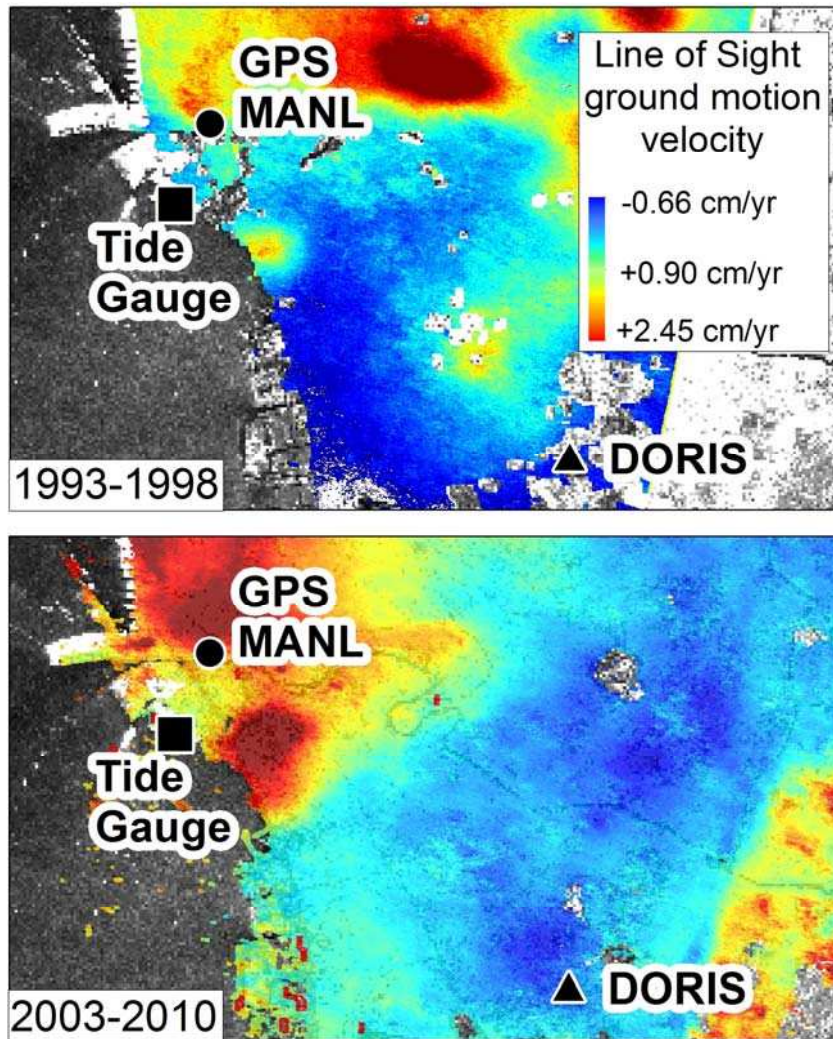
421
 422 *Figure 9: Observed DORIS (MANA/MANB) and GPS (PIMO) geocentric vertical displacements with respect*
 423 *to the international reference frame. DORIS (blue before 2003, green after) and GPS (orange) position time*
 424 *series are shown. Both stations were affected by uplift phenomena with similar rates. MANA and MANB*
 425 *refer to successive DORIS instruments located at the same location (details on the instruments at [doris.org/network/sitelogs.html](http://ids-</i>

 426 <i><a href=)).*
 427



428

429 *Figure 10: Tide-gauge subsidence in the geocentric international terrestrial reference frame based on the*
430 *difference between sea level derived from altimetry (AVISO data) and that from tide-gauge measurements.*
431



432
433 *Figure 11: Close-up images showing Line of Sight ground motion velocity maps (cm/yr) close to the tide*
434 *gauge. The deformation reference was chosen according to the DORIS measurements. Although ground*
435 *motions affecting the location of geodetic instruments are much smaller than in other parts of Manila, they*
436 *are still sufficient to alter the measurements of the tide gauge significantly, thus calling into question its use*
437 *before 1993 for sea-level estimation studies.*

438
439 **4.2 Implications for estimation of sea-level variation from TG measurements**
440 Because sea-level rise exhibits significant regional variability (e.g., Meyssignac & Cazenave, 2012), one
441 critical issue for better estimation of past sea level before the altimetry era (1993) is the analysis of long-

442 term tide-gauge records. This question is particularly significant because there is a disagreement between
443 sea-level budgets as estimated (1) from tide gauges and (2) through independent evaluations of
444 thermosteric and continental ice-melting contributions (Munk, 2002).

445 Tide gauges measure sea level with respect to the land upon which they are grounded (local datum), while
446 global sea level refers to a geocentric reference frame. In other words, both the land and the sea can move
447 with respect to a geocentric reference frame. In practice, vertical ground motions can be removed from
448 tide-gauge measurements using a nearby GPS permanent station (e.g., Wöppelmann *et al.*, 2007),
449 assuming that (1) the tide gauge and the GPS station follow the same vertical motion and (2) that the
450 deformation is linear. Under such conditions, extrapolation of the linear trend of ~10-years GPS time series
451 is valuable to estimate past land motion for at least 50 years. If the differential movements affecting the
452 instruments remained linear, advanced techniques such as PSI could be used as supplemental data to
453 reach the accuracy required of (~ 0.5 mm/yr) and subsequently to assess estimates of global sea-level rise
454 (approximately 1.7 mm/yr between 1950 and 2010, Wöppelmann *et al.*, 2013)

455
456 However, the results reported here show that none of the requirements necessary to estimate geocentric
457 sea-level rise from GPS-corrected tide-gauge data is fulfilled in the case study of Manila. Therefore, this
458 method cannot be used here because of highly variable ground motion. Moreover, the spatial and temporal
459 variability of the surface motion, affecting both the tide gauge and the reference GPS, prevents any
460 extrapolation from corrected gauge time series over the past 50 years. If the differential motion between the
461 GPS and the tide gauge can be estimated for the period monitored by the space-borne radar sensor, the
462 current motion is not representative of past motion (previous to the satellite era). In addition, if the area of
463 maximum subsidence, initially located in Malaboon city, migrates southward, the tide-gauge area could be
464 affected by increased subsidence in the future.

465
466
467 This study encourages DInSAR monitoring at locations where long-term tide-gauge time series are
468 corrected using a distant permanent GPS to verify whether the typical assumptions used to combine the
469 datasets and to estimate geocentric sea-level variation are applicable.

470

471 5. Conclusions

472

473 Subsidence in coastal cities has many effects, potentially ranging from increased frequency of flooding to
474 damage to buildings. In the specific context of Manila, this study has provided the following responses to
475 the questions raised in the introduction:

476

477 (1) What was the spatial and temporal variability of ground-surface deformations in Manila from 1993
478 to 2010? This study has presented evidence for high rates of spatially and temporally variable
479 ground deformation in the Manila urban area (Philippines) based on space-borne SAR
480 interferometry during the last two decades. Displacements up to 15 cm/yr with temporal and spatial
481 variability have been observed. These ground motions are very likely related to groundwater
482 pumping because the Manila urban area is known to be affected by subsidence due to intensive
483 groundwater extraction (Clemente *et al.*, 2001) and due to ground motion along the fault. Although
484 the origin of this latter motion could be tectonic, it is suggested here that the observed ground
485 motion along the fault is actually likely to be related to groundwater pumping as well (except on the
486 Sucat-Binan segment).

487 (2) To which extent do these deformations affect the locations of the tide gauge, the GPS stations, and
488 the DORIS stations? Observed ground motions affect the locations of several geodetic instruments
489 and therefore alter the potential of using their time series to understand past sea levels.

490 (3) What are the possibilities for using sea-level time series before 1993 in Manila? The Manila tide-
491 gauge time series cannot be corrected from its own motion for long-term sea-level estimation on
492 the basis of existing GPS data because the GPS station also experiences variable subsidence and
493 cannot therefore provide an estimate of the deformation occurring during the entire duration of the
494 TG record (the last century).

495

496 From a methodological point of view, this study provides an example of a site where InSAR is helpful in
497 assessing city-scale subsidence or uplift as well as the related consequences for measurements obtained
498 from geodetic instruments located in the city. Because of its deformation characteristics (location, extent,
499 and variable temporal evolution), the Manila metropolitan area has been revealed to be a challenging test
500 site both for application of deformation-monitoring techniques and for surface deformation-related risk
501 management. The approach proposed in this study could enable assessment of the usability of a number

502 of tide gauges suspected of having been affected by local ground motions and finally could provide help in
503 estimating sea-level evolution over the past century.

504

505

506 ACKNOWLEDGEMENTS

507 The work presented in this article was supported by the French National Research Agency (ANR) through
508 the CEP-2009 program (“Coastal environmental changes: impact of sea level rise” (CECILE) project under
509 grant number ANR-09-CEP-001-01). The SONEL data assembly center supported by INSU/CNRS is also
510 acknowledged for providing comprehensive access to GPS data and metadata. We also thank the
511 European Space Agency for providing data and four anonymous reviewers for their constructive comments.

512

513 REFERENCES

514 Ayoub, F., Leprince S., & Keene, L. (2009). *User’s Guide to COSI-CORR Co-registration of Optically*
515 *Sensed Images and Correlation*, Pasadena: California Institute of Technology
516 (http://www.tectonics.caltech.edu/slip_history/spot_coseis/pdf_files/cosi-corr_guide.pdf)

517 Bock, Y., Wdowinski, S., Ferretti, A., Novali, F., & Fumagalli, A. (2012). Recent subsidence of the Venice
518 Lagoon from continuous GPS and interferometric synthetic aperture radar. *Geochemistry Geophysics*
519 *Geosystems*, in press, doi:10.1029/2011GC003976.

520 Brooks, B.A., Merrifield, M.A., Foster, J., Werner, C.L., Gomez, F., Bevis, M., & Gill, S. (2007). Space
521 geodetic determination of spatial variability in relative sea level change, Los Angeles basin. *Geophysical*
522 *Research Letters*, 34, L01611.

523 Clemente, R., Tabios, G., Abracosa, R., David, C., & Inocencio, A. (2001). Groundwater supply in Metro
524 Manila: distribution, environmental and economic assessment. *Discussion Paper Series*, 2001–2006,
525 Makati: Philippine Institute for Development Studies.

526 Chaussard, E., Amelung, F., Abidin, H., & Hong, S.H. (2013). Sinking cities in Indonesia: ALOS PALSAR
527 detects rapid subsidence due to groundwater and gas extraction. *Remote Sensing of the Environment* 128,
528 150-161.

529 Cigna, F., Osmanoglu, C., Cabral-Cano, E., Dixon, T., Ávila-Olivera, J., Garduño-Monroy, V., DeMets, C.,
530 & Wdowinski, S. (2012). Monitoring land subsidence and its induced geological hazard with Synthetic
531 Aperture Radar Interferometry: a case study in Morelia, Mexico, *Remote Sensing of Environment*, 117,
532 146–161.

533 Daag, A., Bacolcol, T., Monstes, A., Kawai, M., & Tsutsui, K. (2011). Use of differential interferometry to
534 monitor ground deformation of Mayon Volcano and land subsidence north of Metro Manila and Bulacan.
535 *Proceedings, 24th Annual Geological Convention of the Geological Society of the Philippines*, Quezon City,
536 December 8–9, 2011.

537 Ferretti, A., Prati, C., & Rocca, F. (2001). Permanent scatterers in SAR interferometry. *IEEE Transactions*
538 *on Geoscience and Remote Sensing* 39(1), 8–20.

539 Hanson, S., Nicholls, R., Ranger, N., Hallegatte, S., Corfee-Morlot, J., Herweijer, C., & Chateau, J. (2011).
540 A global ranking of port cities with high exposure to climate extremes. *Climatic Change* 104, 89–111.

541 Hanssen, R. (ed.) (2001). *Radar Interferometry: Data Interpretation and Error Analysis*, Dordrecht: Kluwer
542 Academic.

543 IOC (2012). *The Global Sea Level Observing System Implementation Plan 2012*. Intergovernmental
544 Oceanographic Commission, Technical Series No. 100.

545 Jacinto, G., Azanza, R., Velasquez, I., & Siringan, F. (2006). Manila Bay: environmental challenges and
546 opportunities. In: *Environment in Asia Pacific Harbors*, 309-328, Dordrecht: Springer.

547 Kim, S., Wdowinski, S., Dixon, T., Amelung, F., Kim, J., & Won, J. (2010). Measurements and predictions
548 of subsidence induced by soil consolidation using persistent scatterer InSAR and a hyperbolic model.
549 *Geophysical Research Letters* 37, L05304 .

550

551 Lagios, E., Parcharidis, I., Sakkas, V., Raucoules, D., Feurer, D., Le Mouelic, S., King, C., Carnec, C.,
552 Novali, F., Ferretti, A., Capes, R., & Cooksley, G., (2006). Subsidence monitoring within the Athens basin
553 using advanced space radar interferometric techniques. *Earth, Planets, and Space* 58, 505–513.

554 Le Mouelic, S., Raucoules, D., Carnec, C., & King, C. (2005). A least-squares adjustment of multi-temporal
555 InSAR data: application to the ground deformation of Paris. *Photogrammetric Engineering and Remote*
556 *Sensing* 71, 197–204.

557 Leprince, S., Ayoub, F., Klingner, Y., & Avouac, J. (2007). Co-registration of optically sensed images and
558 correlation (COSI-Corr): an operational methodology for ground-deformation measurements. *Proceedings,*
559 *IEEE International Geoscience and Remote Sensing Symposium (IGARSS 2007)*, Barcelona, July 2007.

560 Massonnet, D. , & Feigl, K. (1998). Radar interferometry and its application to changes in the Earth's
561 surface. *Reviews of Geophysics* 36(4), 441–500.

562 Meysignac, B., & Cazenave, A. (2012). Sea level: A review of present-day and recent past changes and
563 variability. *Journal of Geodynamics* 58, 96–109.

564 Munk, W. (2002). Twentieth-century sea level: an enigma. *Proceedings of the National Academy of*
565 *Sciences of the United States of America* 99, 6550–6555.

566 National Statistics Office of the Republic of the Philippines (2010). 2010 Census of Population and
567 Housing, National Capital Region. Available at :
568 [http://www.census.gov.ph/sites/default/files/attachments/hsd/pressrelease/National Capital Region.pdf](http://www.census.gov.ph/sites/default/files/attachments/hsd/pressrelease/National%20Capital%20Region.pdf).

569 Pepe, A., Sansosti, E., Berardino, P., & Lanari, R. (2005). On the generation of ERS/ENVISAT DInSAR
570 time series via the SBAS technique. *IEEE Geoscience and Remote Sensing Letters* 2(3), 265–269.

571 Peltzer G., Crampé F., Henley, S., & Rosen P.(2001). Transient strain accumulation and fault interaction in
572 the Eastern California shear zone, *Geology*, 29: 975-978

573 Raucoules, D., Bourguin, B., De Michele, M., Le Cozannet, G., Closset, L., Bremmer, C., Veldkamp, H.,
574 Tragheim, D., Bateson, L., Crosetto, M., Agudo, M., & Engdahl, M. (2009). Validation and intercomparison
575 of Persistent Scatterers Interferometry: PSIC4 project results. *Journal of Applied Geophysics* 68, 335–347.

576 Raucoules, D., Parcharidis, I., Feurer, D., Novalli, F., Ferretti, A., Carnec, C., Lagios, E., Sakkas, V., Le
577 Mouelic, S., Cooksley, G., & Hosford, S. (2008). Ground deformation detection of the greater area of

578 Thessaloniki (Northern Greece) using radar interferometry techniques. *Natural Hazards and Earth System*
579 *Sciences* 8, 779–788.

580 Rimando, R., & Knuepfer, P. (2006). Neotectonics of the Marikina Valley Fault system (MVFS) and tectonic
581 framework of the structures in northern and central Luzon, Philippines. *Tectonophysics* 415, 17–38.

582 Rodolfo, K.S., & Siringan, F.P. (2006). Global sea-level rise is recognized, but flooding from anthropogenic
583 land subsidence is ignored around northern Manila Bay, Philippines. *Disasters* 30, 118–139.

584 Santamaría-Gómez, A., Gravelle, M., Collilieux, X., Guichard, M., Miguez, B.M., Tiphaneau, P., &
585 Wöppelmann, G. (2012). Mitigating the effects of vertical land motion in tide gauge records using a state-of-
586 the-art GPS velocity field. *Global and Planetary Change* 98–99, 6–17.

587 Siringan, F.P., & Ringor, C.L. (1998). Changes in bathymetry and their implications for sediment, dispersal
588 and rates of sedimentation in Manila Bay. *Science Diliman* 10(2), 12–26.

589

590 Tandanand, S., & Powell, R. (1991). Determining horizontal displacement and strain due to subsidence.
591 Washington D.C.: U.S. Dept. of the Interior, Bureau of Mines.

592

593 Usai, S. (2003). A least-squares database approach for SAR interferometric data. *IEEE Transactions on*
594 *Geoscience and Remote Sensing* 41(4), 753–760.

595

596 Volkov, D.L., Larnicol, G., & Dorandeu, J. (2007). Improving the quality of satellite altimetry data over
597 continental shelves. *Journal of Geophysical Research* 112, C06020.

598 Williams, S.D.P. (2008). CATS: GPS coordinate time series analysis software. *GPS Solutions* 12(2), 147–
599 153.

600 Willis, P., Fagard, H., Ferrage, P., Lemoine, F.G., Noll, C.E., Noomen, R., Otten, M., Ries, J.C., Rothacher,
601 M., Soudarin, L., Tavernier, G., & Valette, J.J. (2010). The International DORIS Service: toward maturity.
602 In: DORIS: Scientific Applications in Geodesy and Geodynamics, *Advances in Space Research*
603 45(12):1408–1420.

604 World Bank (2010). Climate risk and adaptation in Asian Coastal Megacities: a synthesis report. 97p.,
605 available at : [http://siteresources.worldbank.org/EASTASIAPACIFICEXT/Resources/226300-](http://siteresources.worldbank.org/EASTASIAPACIFICEXT/Resources/226300-1287600424406/coastal_megacities_fullreport.pdf)
606 [1287600424406/coastal_megacities_fullreport.pdf](http://siteresources.worldbank.org/EASTASIAPACIFICEXT/Resources/226300-1287600424406/coastal_megacities_fullreport.pdf).

607 Wöppelmann, G., Miguez, B.M., Bouin, M.N., & Altamimi, Z. (2007). Geocentric sea-level trend estimates
608 from GPS analyses at relevant tide gauges world-wide. *Global and Planetary Change* 57, 396–406.

609 Wöppelmann, G., Le Cozannet, G., de Michele, M., Raucoules, D., Cazenave, A., Garcin, M., Hanson, S.,
610 Marcos, M., & Santamaría-Gómez A. (2013). Is subsidence increasing the exposure to sea level rise
611 impacts in Alexandria, Egypt? *Geophysical Research Letters* 40, 1-5.

612 Wegmuller, U., Werner, C., & Strozzi, T., (1998). SAR interferometric and differential interferometric
613 processing chain. *Proceedings, International Geoscience and Remote Sensing Symposium (IGARSS)*, 2,
614 1106–1108, July 1998, Seattle.

615

616 Wright, T., Parsons, B., & Lu, Z. (2004). Towards mapping surface deformation in three dimensions using
617 InSAR. *Geophysical Research Letters* 31(1), L01607.

618

619 Zebker, H., Rosen, P., & Hensley, S. (1997). Atmospheric effects in interferometric synthetic aperture radar
620 surface deformation and topographic maps, *Journal of Geophysical Research: Solid Earth* – B2 102, 2156-
621 2202

622